



# Aggregate shape determination via light scattering by aligned and randomly oriented polydisperse aggregates

George W. Mulholland<sup>a</sup>, James Corson<sup>b,\*</sup>, Michael R. Zachariah<sup>a,c</sup>

<sup>a</sup> Department of Chemical and Biomolecular Engineering, University of Maryland, College Park, MD, USA

<sup>b</sup> U.S. Nuclear Regulatory Commission, Rockville, MD, USA

<sup>c</sup> Department of Chemistry and Biochemistry, University of Maryland, College Park, MD, USA



## ARTICLE INFO

### Article history:

Received 7 June 2018

Revised 27 July 2018

Accepted 27 July 2018

Available online 30 July 2018

## ABSTRACT

We present calculations of light scattered by simulated aligned and randomly oriented fractal aggregates of touching spheres. The alignment by an applied electric field is in the direction yielding the minimum energy associated with the polarizability of the aggregate. This direction is also within a few degrees of the direction associated with the smallest inertial eigenvalue. Aggregates were generated to have a fractal dimension of 1.78 (characteristic of diffusion-limited cluster-cluster aggregation) and to simulate the range of aggregate sizes (30 to 2000) and size distributions for post-flame generated soot by a range of hydrocarbon fuels. More nearly monodisperse aggregates were also generated to simulate the size distributions obtained via mobility or mass classification. We show that a ratio of slopes computed from small angle light scattering intensities (Guinier plots) is related to the shape parameter  $A_{31}$ , which is the ratio of the largest to the smallest principle radii of gyration of the inertia tensor. A geometric interpretation of the overall shape is presented based on the semi-axes of an ellipsoid. Results on the correlation between the maximum structure factor ratio  $\{S(q)\}_a / \{S(q)\}_r$  for the monodisperse and polydisperse clusters and the average value of  $A_{31}$  indicate that light scattering measurements in the  $q$  range of fractal behavior would also be feasible for shape characterization. Our calculations indicate that light scattering measurements have a good potential for characterizing aggregate shape with an advantage of being more sensitive to shape than mobility measurements.

Published by Elsevier Ltd.

## 1. Introduction

Aerosol aggregates are generated by building fires and wild-land fires; by high temperature processes such as diesel engines, smelters, and pulverized coal combustion; and in the production of fine particles including carbon black, fumed silica, and titania [8]. It has been found that the morphology of aerosol aggregates formed by such processes can be described by the equation:

$$N = k_0 (R_g/a)^{d_f}, \quad (1)$$

where  $d_f$  is the fractal dimension,  $N$  is the number of spheres in the aggregate,  $R_g$ , the aggregate radius of gyration, and  $a$  the radius of the primary spheres. For this study, the primary sphere radius is assumed to be the same for every sphere in a given aggregate.

Theoretical and experimental studies have demonstrated the importance of the fractal dimension in describing the transport (diffusion, electrical mobility, phoretic processes), aggregate

growth (diffusion limited cluster-cluster aggregation), and optical properties including the  $q$  dependence of light scattering [31]. There has been relatively little research characterizing the overall shape of aggregates other than measurements by electron microscopy. The simulation results presented here suggest that light scattering measurements from aligned and randomly oriented aggregates can be used to determine the shape parameters for both monodisperse and polydisperse aggregates.

While there have not been many experimental studies of the shape parameter, there have been a number of studies of aggregate alignment in a strong field. The aggregates become aligned in an orientation that minimizes their energy in the field [10,20]. This effect has been demonstrated experimentally by placing aggregates in an external electric field and measuring changes in scattered light intensity [3,5,29] or electrical mobility [16,19,21,30] as the field strength changes. Calculations of electrical mobility versus field strength based on an extended Kirkwood Riseman theory [6] are in good agreement with published experimental data for soot [21], which show an increase in mobility on the order of 8% from random to aligned orientations. Filtration is another area where aggregate alignment could be important. Chen et al. [4] ob-

\* Corresponding author.

E-mail address: [James.Corson@nrc.gov](mailto:James.Corson@nrc.gov) (J. Corson).

served as much as a factor of 1.6 higher penetration of silver aggregates relative to silver spheres with the same mobility with increasing face velocity to the filter. They attribute the higher penetration to increased alignment which might result from the increased velocity gradient in the 1  $\mu\text{m}$  pore of the Nucleopore filters.

There have been several studies of aggregate shape based on computer simulations. Fry et al. [9] computed the shape anisotropy for simulated clusters carrying out off-lattice Monte Carlo simulations for diffusion-limited cluster-cluster aggregation (DLCA) with up to  $3 \times 10^6$  monomers. The shape anisotropy is defined in terms of ratio of the squares of the largest to smallest principle radii of gyration,  $A_{31}$ , and in terms of the semi major axes ( $a, b, c$ ) of the corresponding ellipsoid. We will use the same characterization of shape in our study. They obtain average values of 3.70 and 3.09 for  $A_{31}$  and  $c/a$  for the dilute limit corresponding to a cluster volume fraction less than about 0.1. The shape anisotropy distribution is asymmetric, extending out to values as large as 15 with, apparently, an exponential decay for large  $A_{31}$ .

Heinson et al. [13] carried out DLCA calculations similar to those of Fry et al. and computed the structure factor  $S(q)$  in addition to  $A_{31}$  for each aggregate. In their analysis, they assumed a pair correlation function that depends on only the radial distance between all the spheres in the aggregate with the following form:

$$g(r) = Cr^{d_f-3} \exp\left(-\left(r/\xi\right)^\gamma\right) \quad (2)$$

The cutoff function includes a so called stretching exponent  $\gamma$ . From the functional relationship between  $S(q)$  and  $g(r)$ , Heinson et al. obtained a correlation between the value of  $A_{31}$  for each cluster and the best fit value of  $\gamma$  for each cluster. The authors point out that the value of the exponent  $\gamma$  can serve as a shape factor in place of  $A_{31}$ . Heinson et al. [13] also show that the value of the fractal prefactor  $k_0$  determined for each cluster is correlated with each value of  $A_{31}$ .

Lindsay et al. [22] also carried out DLCA simulations and characterized the aggregate anisotropy by expanding the orientation averaged structure factor in terms of spherical harmonics. The largest term in expansion shifted to a larger order spherical harmonics with increasing value of  $q$ . The normalized  $S(q)$  was found to be independent of aggregate size (scale invariant) for DLCA clusters. One important application of their analysis was the calculation of the contribution of rotational diffusion to quasielastic light scattering.

Mulholland et al. [25] generated fractal aggregates using the DLCA code developed by Heinson and computed  $A_{31}$  and  $S(q)$  for both randomly oriented and aligned clusters. The slopes of  $1/S(q)$  vs  $q^2$  were computed for small  $q$  for both orientations. A strong correlation was obtained between the ratio of the random orientation slope to the aligned orientation slope and the value of  $A_{31}$  for the aggregate. The light scattering intensity integrated over an angle range between about  $7^\circ$  and  $173^\circ$  for simulated soot aggregates with 300 primary spheres was computed for both the random and aligned orientation. The ratio of the intensity for the two orientations, about 2, was in qualitative agreement with experiments [5,29]. The magnitude of the effect suggested that such measurements could be useful for studying the presence of soot as well as changes in the shape of the soot particles.

The current study is an extension of the previous study by Mulholland et al. [25] to include the effect of polydispersity on the shape anisotropy inferred for small and large  $q$ , to quantify the alignment direction of the aggregates, and to display the shape information graphically. A significant motivation for this study is the much larger effect of alignment on the light scattering intensity compared to the electrical mobility. To provide more realistic simulation results, two size distributions close to those observed ex-

perimentally were considered: A nearly monodisperse size distribution similar to that obtained by size selection based on electrical mobility or mass [26] and a large polydispersity such as observed in soot from buoyant turbulent diffusion flames [17].

In the previous study, it was assumed that the alignment direction was along the principal axes of the inertia tensor. However, the aggregates are aligned in the direction corresponding to the lowest polarizability energy of the aggregate. Thus it is the principle axes of the polarizability tensor that control the orientation. In this study, both sets of principal axes are determined. Also, in the previous study, the power law slope for the large  $q$  behavior for the aligned aggregate was about  $-3.0$  for a 1000 sphere aggregate compared to a value of  $-1.78$  for the random orientation. The generality of this initial observation will be assessed.

A fundamental difference from the previous studies is that the calculation of the aligned  $S(q)$  from the pair correlation function requires the vector pair correlation function. Previous studies mentioned above [9,13,22] are based on an average over all orientations, which leads to a scalar pair correlation function.

## 2. Theory

The prediction of the effect of orientation on the light scattering by clusters is based on computing the orientation of the cluster in the electric field together with the calculation of the structure factor. Both of these topics have been explored in previous publications [6,20,21] so only a brief summary of the key results will be presented. A key element of this study is including the effect of the polydispersity of the cluster distribution for providing results relevant to both flame-produced aggregates and to size classified aggregates studied in the laboratory. The equations previously derived for single aggregates are modified for application to polydisperse aggregates. The limit of small  $q$  is of special interest for assessing the shape of the aggregates and the analysis given by Mulholland et al. [25] is extended to include this case.

### 2.1. Alignment

The probability distribution of a particle's orientation in an electric field is given by the Boltzmann distribution [10],

$$f(\phi, \theta, \psi) = \frac{e^{-U/kT}}{\int_0^{2\pi} \int_0^\pi \int_0^{2\pi} e^{-U/kT} \sin\theta d\phi d\theta d\psi} \quad (3)$$

where  $U$  is the energy of the particle in the electric field for the particle orientation given by the Euler angles ( $\phi, \theta, \psi$ ). As shown in Corson et al. [6], we can explicitly write the interaction energy of a cluster in an electric field  $\vec{E}$  as

$$U = -\frac{1}{2} (\sin^2\psi \sin^2\theta \alpha_1 + \cos^2\psi \sin^2\theta \alpha_2 + \cos^2\theta \alpha_3) E^2 \quad (4)$$

where  $\alpha_3 > \alpha_2 > \alpha_1$  are the eigenvalues of the polarizability tensor. The lowest energy corresponds to  $\theta = 0$ . Eq. (4) assumes that the particle is perfectly conducting, which is reasonable even for aerosol particles composed of non-conducting materials due to their small size and the presence of contaminants [10]. In this analysis, we assume the electric field is either strong enough that the cluster is fully aligned or weak enough for all orientations to be equally probable. We obtain the polarizability tensor for each particle in this study using the ZENO code [24], which uses a random walk algorithm to compute various properties of a particle consisting of spherical subunits. We then determine the eigenvalues and eigenvectors of the polarizability tensor and choose our body-fixed coordinates for each particle such that the  $x$ - and  $z$ -axes correspond to directions (i.e. eigenvectors) associated with the largest and smallest eigenvalues, respectively.

**Table 1**

Angle between the eigenvectors corresponding to the minimum eigenvalue of the inertia tensor and the maximum eigenvalue of the polarizability tensor for 20 isomers for each value of  $N$ . In all cases, the fractal dimension and prefactor are 1.78 and 1.3, respectively.

$N$	Minimum angle	Maximum angle	Average angle	Standard deviation
26	0.20	13.82	4.01	3.56
55	0.46	5.96	2.58	1.76
99	0.73	6.55	2.77	1.76
197	0.16	8.53	2.13	1.97
402	0.32	12.92	2.83	2.77
800	0.91	7.86	3.05	1.79
1946	0.58	4.36	2.03	0.98

Another alignment direction of interest in regard to small angle scattering, is the direction of the smallest principal radius of gyration of the inertia tensor for the aggregates. As indicated in Table 1 for clusters ranging from 26 spheres to 1946 spheres, the direction of the lowest dipole-field interaction energy and the direction associated with the smallest inertial eigenvalue are typically within a few degrees. Exceptions to this rule occur for particles that are fairly isotropic, such that the eigenvectors of the polarizability tensor are more sensitive to uncertainty in the ZENO calculations than more elongated particles. Note that in this study, we only use the inertia tensor to calculate the parameter  $A_{31}$ , which can be thought of as a measure of particle shape. (See Supplementary Material, available online, for more detailed information about the difference between the inertia and polarizability tensor eigenvectors.)

## 2.2. Scattering cross section for aggregates

The structure factor of an aggregate of touching spheres in the Rayleigh–Gans–Debye limit can be written as:

$$S(\vec{q}, \vec{\phi}, N) = N^{-2} \sum_{i,j} e^{i\vec{q} \cdot (\vec{r}_i - \vec{r}_j)}, \quad (5)$$

where  $N$  is the number of spheres in the cluster and  $\vec{\phi}$  represents a set of Euler angles for the initial orientation of the cluster relative to the space fixed axes located at the center of mass of the cluster. The orientation averaged structure factor is expressed as  $\langle S(\vec{q}, N) \rangle_{or}$  where either random orientation (subscript  $r$ ) or aligned orientation (subscript  $a$ ) are considered here. In the generation of clusters of  $N$  primary spheres, more than one structure is formed and the “isomer” number is referred to as  $i$  with the maximum value  $i_s$ .

The differential cross section of the orientation averaged cluster per isomers is given by:

$$\left\langle \frac{d\sigma^{agg}(\vec{q}, N)}{d\Omega} \right\rangle_{or} = \frac{d\sigma^R}{d\Omega} N^2 \sum_{i=1}^{i_m} \frac{\langle S(\vec{q}, N, i) \rangle_{or}}{i_m}, \quad (6)$$

where the Rayleigh differential scattering cross section,  $\sigma^R$ , is expressed in terms of the refractive index  $m$ , the radius of the primary sphere  $r$ , and the wave number  $k$ .

$$\frac{d\sigma^R}{d\Omega} = k^4 r^6 \left| \frac{m^2 - 1}{m^2 + 2} \right|^2 \quad (7)$$

This cross section corresponds to the polarization direction of the incident light being perpendicular to the scattering plane. It is convenient to use a reduced version of the differential cross section expressed by:

$$H_{or}(\vec{q}, N) = \left\langle \frac{d\sigma^{agg}(\vec{q}, N)}{d\Omega} \right\rangle_{or} / \frac{d\sigma^R}{d\Omega} \quad (8)$$

For a polydisperse distribution of aggregates with fraction  $f(N)$  of aggregates with  $N$  primary spheres, the reduced cross section

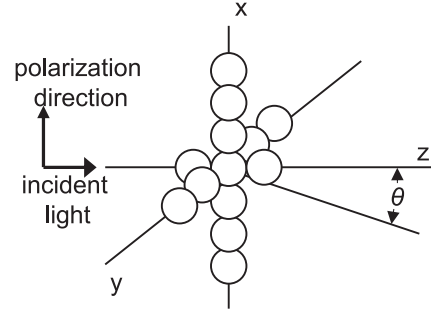


**Fig. 1.** Schematic of light scattering geometry with the  $z$ - $y$  plane the scattering plane. The orientation of a simple cluster with the major principal axis along the  $x$ -direction and the minor principal axis in the  $z$ -direction is shown.

is

$$\begin{aligned} H_{or,p} &= \int_{N_{\min}}^{N_{\max}} \left( \sum_{i=1}^{i_m} f(N) N^2 \frac{\langle S(\vec{q}, N, i) \rangle_{or}}{i_m} \right) dN \\ &= \int_{N_{\min}}^{N_{\max}} f(N) H_{or}(N) dN \end{aligned} \quad (9)$$

The polydispersity relates to the number of primary spheres in the aggregate and not to the size of the primary spheres, which are all assumed to have the same diameter. In this analysis, it is assumed that the aggregates are far enough apart that there is no multiple scattering among aggregates. This is the quantity that can ultimately be compared with experimental data.

## 2.3. Limit of small $q$

As shown in Mulholland et al. [25], the orientation averaged structure factor in the small  $q$  limit for a single aggregate is given by

$$\langle S(\vec{q}, N) \rangle_r = 1 - \frac{1}{3} q^2 (R_g(N))^2, \quad \text{for random orientation} \quad (10)$$

$$\langle S(\vec{q}, N) \rangle_a = 1 - \frac{1}{2} q^2 (Y^2 + Z^2)^2 = 1 - \frac{1}{2} q^2 (R_1^2)^2, \quad \text{for aligned orientation} \quad (11)$$

where  $Y^2 = \sum y_i^2 / N$  and  $R_1^2$  the principle radius of gyration about the  $x$ -axis, which corresponds to the principal axis of the polarizability tensor. The incident light is in the  $z$ -direction while the electric field is in the  $x$ -direction (Fig. 1). Eq. (10) is a well known result [12] and Eq. (11) is a consequence of only the  $y$  components of the particle coordinates contributing to the light scattering in the small angle limit. Of course,  $Z^2$  appears because we are rotating around the  $x$ -axis; if we had a fixed orientation, then only  $Y^2$  would appear. Averaging over the isomers for the aligned orienta-

tion gives:

$$\sum_{i=1}^{i_m} \frac{\langle S(\vec{q}, N, i) \rangle_a}{i_m} = 1 - \frac{1}{2} q^2 \langle (R_1(N))^2 \rangle_i \quad (12)$$

For the case of random orientation, the value of  $R_g(N)$  is independent of the isomer number because of the way the aggregates are generated: for the user-specified number of spheres  $N$ , fractal dimension  $d_f$ , and prefactor  $k_0$ , the  $(x, y, z)$  coordinates of each sphere have been generated using the Mackowski algorithm [23].

Substituting Eq. (10) for the random orientation and Eq. (12) for the aligned orientation into Eq. (9), the following expressions are obtained for the reduced light scattering cross section for polydisperse aggregates with isomers:

$$H_{r,p}(q) = \int_{N_{\min}}^{N_{\max}} f(N) N^2 \left( 1 - \frac{1}{3} q^2 \langle R_g(N)^2 \rangle \right) dN = \langle N^2 \rangle \left( 1 - \frac{1}{3} q^2 R_{g,2}^2 \right). \quad (13)$$

Here,

$$\langle N^2 \rangle = \int_{N_{\min}}^{N_{\max}} f(N) N^2 dN \quad (14)$$

$$R_{g,2}^2 = \left( \int_{N_{\min}}^{N_{\max}} f(N) N^2 R_g^2(N) dN \right) / \langle N^2 \rangle \quad (15)$$

The subscript 2 regarding the radius of gyration refers to the  $N^2$  term in the sum.

The corresponding expression for the aligned orientation is given by

$$H_{a,p}(q) = \int_{N_{\min}}^{N_{\max}} f(N) N^2 \left( 1 - \frac{1}{2} q^2 \langle (R_1(N))^2 \rangle_i \right) dN = \langle N^2 \rangle \left( 1 - \frac{1}{2} q^2 R_{1,2}^2 \right). \quad (16)$$

$$\text{where } R_{1,2}^2 = \left( \int_{N_{\min}}^{N_{\max}} f(N) N^2 \langle (R_1(N))^2 \rangle_i dN \right) / \langle N^2 \rangle \quad (17)$$

In Eq. (17), an average over the isomers for a given value of  $N$  is computed first before averaging over the values of  $N$ . This approach is valid because there are the same number of isomers for every aggregate size.

From the 1st two terms of the Taylor expansion of the inverses of Eq. (13) and (16) for small  $q$ , one obtains:

$$\frac{\langle N^2 \rangle}{H_{r,p}} = 1 + \frac{1}{3} q^2 R_{g,2}^2 \quad (18)$$

$$\frac{\langle N^2 \rangle}{H_{a,p}} = 1 + \frac{1}{2} q^2 R_{1,2}^2 \quad (19)$$

These equations are in the form for Zimm plots of the inverse of the intensity versus the square of the appropriate radius of gyration. It is of interest to look at the correlation between the ratio of slopes for  $1/H_q$  vs  $q^2$  (for the random and aligned orientations) and the average of  $A_{31}$ , which is the ratio of the largest to the smallest principal radii of gyration. A strong correlation was observed in a previous study for monodisperse aggregates [25]. For a polydisperse distribution, the calculated slope ratio from the Rayleigh–Gans–Debye calculations should match the theoretical slope ratio,

$$\text{SR} = \frac{2 R_{g,2}^2}{3 R_{1,2}^2} \quad (20)$$

To facilitate comparison between the slope ratio and  $A_{31}$  for a distribution of particles, we define the average  $A_{31}$  as the ratio of the average of the largest inertia tensor eigenvalue to the average of the smallest inertia tensor eigenvalue:

$$A_{31} = \frac{R_{3,2}^2}{R_{1,2}^2} \quad (21)$$

Here,  $R_{1,2}^2$  is defined by Eq. (17), while  $R_{3,2}^2$  is defined similarly, with the largest principal radius of gyration replacing the smallest principal radius of gyration in the equation.

### 3. Simulations

For this study, we have calculated the structure factor for particles with fixed, aligned, and random orientations. All particles have been generated using the Mackowski algorithm [23]. All calculations are performed for a wavelength of 630 nm and a primary sphere radius of 15.5 nm. Unless noted otherwise, the particles have fractal dimension and prefactor equal to 1.78 and 1.3, respectively.

The structure factors for a given particle are calculated as follows. First, we write the particle coordinates in terms of the body-fixed axes corresponding to the principal axes of the polarizability tensor. Next, we determine the aligned structure factor by rotating the particle around the major axis and calculating  $S(q)$  for 36 orientations evenly spaced in the interval  $[0, 2\pi]$ .  $S_a(q)$  is the average of the structure factor for these 36 orientations. Finally, we determine the randomly-oriented structure factor  $S_r(q)$  by averaging  $S(q)$  from Eq. (5) for 1000 particle orientations; orientations are chosen in ten-equally spaced bins in the intervals  $[0, 2\pi]$ ,  $[0, 1]$ , and  $[0, 2\pi]$  for  $\phi$ ,  $\cos \theta$ , and  $\psi$ , respectively. The Eulerian transformation tensor [11] is used to calculate the coordinates for the rotated aggregate about one axis for the aligned case and about all three axes for the random orientation.

We have also determined the light scattering intensity for narrow distributions (e.g. from a DMA) and for a broad distribution, such as what one might obtain by sampling from the overfire region of a diffusion flame. For these distributions, the reduced light scattering cross-section from randomly-oriented particles is given by Eq. (13), where  $f(N)$  is the probability density function for the distribution in terms of the number of monomers in a particle. For the narrow (i.e. DMA) distributions, we use a lognormal PDF with  $\sigma_g = 1.08$  and  $N_g$  corresponding to the nominal DMA mobility. (See the Supplemental information – available online – for an explanation of how  $\sigma_g$  is determined.) For the broad distribution, we use a lognormal PDF with  $N_g = 226$  and  $\sigma_g = 3$ , which is representative of overfire soot from turbulent diffusion flames [17].

### 4. Results

#### 4.1. Orientation averaged

The orientation averaged structure factor  $\langle S(\vec{q}, N, i) \rangle_{or}$  for random orientation has the expected power slope of  $-D_f$  ( $-1.78$ ) for aggregates ranging in size from 100 to 2000 as seen in Fig. 2a; however, for the aligned orientation, there is a less well defined power law dependence and an eyeball fit gives a steeper slope in the range of  $-2.5$  to  $-3$  for the larger two clusters. The smaller two aggregates are too small to estimate a power law exponent. This difference in  $q$  dependence was previously presented by Mulholland et al. [25].

#### 4.2. Aggregate “isomers”/Averaging

The results in Fig. 2a are for a single aggregate. Multiple aggregates were generated with the same number of primary sphere. Each one has a different structure with a different set of eigenvalues for the polarizability tensor. The structure factor  $\langle S(\vec{q}, N, i) \rangle_{or}$  is shown in Fig. 3 for 20 isomers for aggregates with 300 spheres and 1000 spheres. There is a much broader band of curves for the aligned orientation compared to the random orientation. For the largest aggregates, there is a broad spread in the structure factors

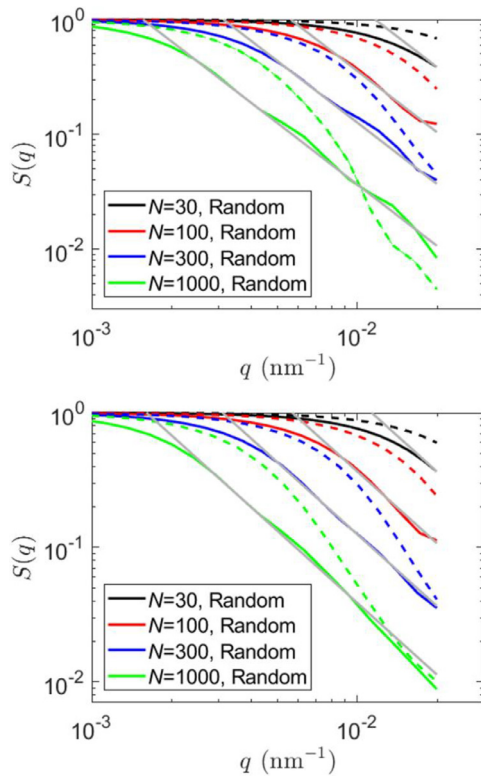


**Fig. 2.** Structure factor vs.  $q$  for aggregates with  $N=30, 100, 300,$  and  $1000$ . Results are shown for single particles (top) and for the averages of 20 isomers (bottom). The solid lines represent the results for the random orientation, while the dashed lines represent the aligned orientation. The solid gray lines are proportional to  $q^{-1.78}$  and are shown for comparison.

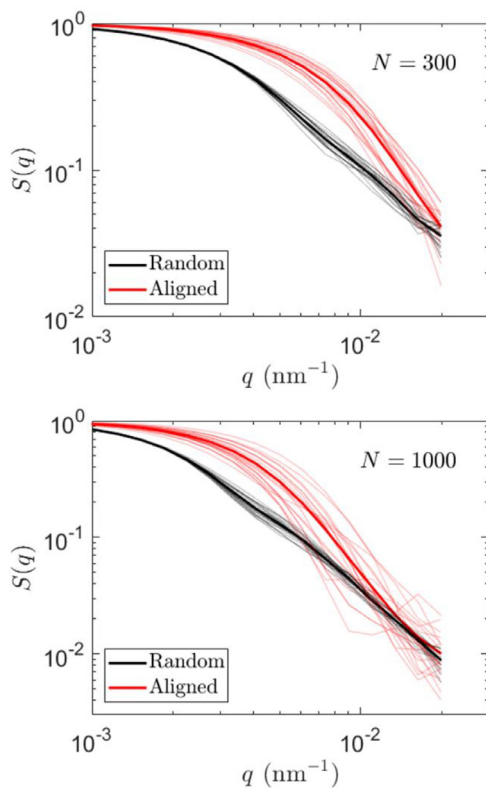


**Fig. 3.** Comparison of  $S(q)$  for random and aligned orientations for 20 isomers with  $N=300$  (top) and  $N=1000$  (bottom). The dark, thick lines represent the average of the 20 isomers.

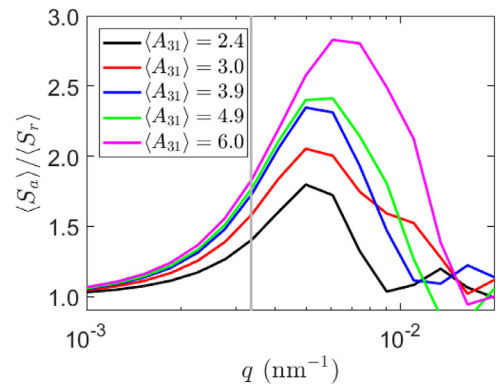


**Fig. 4.** Comparison of the structure factor ratio for 299-sphere aggregates ( $k_0 = 1.3$ ) with different measures of  $A_{31}$ . The 20 isomers with  $N=299$  are binned according to  $A_{31}$ , then the average  $S_a(q)$  and  $S_r(q)$  are calculated for each bin. The grey, vertical line at  $q = 0.0033 \text{ nm}^{-1}$  (corresponding to  $1/R_g$ ) shows that the peaks in the ratios are beyond the Guinier regime.

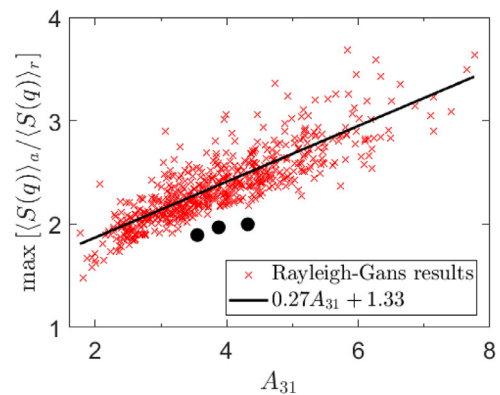


**Fig. 5.** Maximum structure factor ratio (i.e. the peak value in a plot of  $\langle S(q) \rangle_a / \langle S(q) \rangle_r$ ) for all particles in the broad particle size distribution (20 isomers each for 39 aggregate sizes). For comparison, results for the broad cluster size distributions (with  $k_0 = 0.95, 1.3,$  and  $1.83$ ) are shown as solid circles.

likely resulting from differences in short range structure. The average of the 20 isomer values are also plotted in Fig. 3 and for the 4 aggregates sizes shown in Fig. 2. Such averaging occurs in light scattering measurements of aggregates produced by high temperature processes such as soot produced by flames.

#### 4.3. Shape correlations

To assess the relationship between the aggregate shape and the structure factor we have plotted the ratio  $\langle S(q, N, A_{31}) \rangle_a / \langle S(q, N, A_{31}) \rangle_r$  vs  $q$  in Fig. 4 for  $N=299$  and  $k_0 = 1.3$ . The 20 values of the structure factors were binned according to  $A_{31}$  and then the two averages were computed for each bin. It is seen that there is a correlation between the peak slope ratio and the value of  $A_{31}$ . Fig. 5 shows the correlation between the maximum structure factor ratio (i.e. the peak value in a plot of  $\langle S(q) \rangle_a / \langle S(q) \rangle_r$ ) for all particles in the broad particle size distribution (20 isomers each for 39 aggregate sizes) vs.  $A_{31}$  for each aggregate. The results show a positive correlation between the “stringiness” of a particle and the maximum ratio of light-scattering intensity between aligned and random orientations.

#### 4.4. Polydisperse aggregates

The reduced light scattering intensity  $H_{or,p}(q)$ , which is averaged over both the size distribution and isomer distribution, is plotted in Fig. 6 for a lognormal distribution of aggregates ( $N_g = 226$ ,

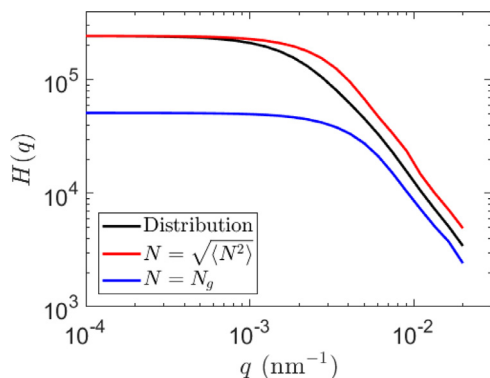


**Fig. 6.** Comparison of monodisperse distribution for two different values of  $N$  (226 and 493) with the results for the polydisperse case ( $N_g=226$  and  $\sigma_g=3$ ).

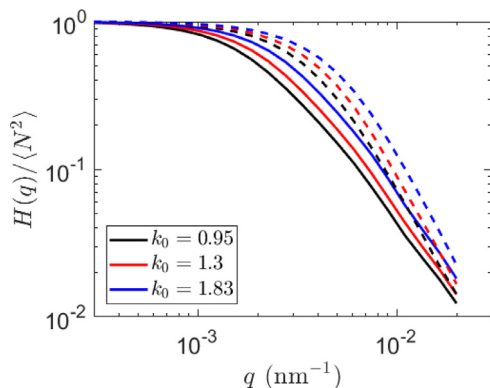


**Fig. 7.** Light scattering intensity from a broad lognormal aggregate size distribution ( $N_g=226$  and  $\sigma_g=3$ ). The solid lines represent the random particle orientation, while the dashed lines represent aligned aggregates. Results are shown for distributions involving aggregates with three different prefactors. For all cases, the fractal dimension is 1.78.

**Table 2**

Fits to the exponential region of the  $H$  vs  $q$  results for broad distributions with various primary sizes and prefactors in the fractal equation. The fits are based on results for  $q > 0.01$ .

Case	$A_{31}$	Fit exponents	
		Random	Aligned
$a = 15.5$ nm, $k_0 = 0.95$	4.32	-1.77	-2.34
$a = 15.5$ nm, $k_0 = 1.3$	3.88	-1.87	-2.44
$a = 15.5$ nm, $k_0 = 1.83$	3.55	-1.86	-2.29

$\sigma_g=3$ ) along with the isomer averaged plots for  $N=226$  and for  $N=[\langle N^2 \rangle]^{1/2}=493$ . In all three cases the large  $q$  slopes are nearly identical. The second choice (i.e.  $N=493$ ) provides a better fit for small  $q$ ; the polydispersity causes the smaller curvature at intermediate  $q$  compared to the monodisperse case. In Fig. 7 it is seen that the slopes at large  $q$  for the random orientation (1.77 to 1.87; see Table 2) are close to the value of 1.78 obtained for the individual aggregates, while the slopes for the aligned cases are larger, about 2.3, though not as large as obtained for individual aggregates. For a fixed  $q$ , the reduced light scattering intensity is smallest for the largest value of  $R_g$ . The smallest value of the prefactor gives the largest  $R_g$  as seen from the fractal equation. This explains the ordering of the intensity curves in Fig. 7.

A more detailed illustration of the effect of shape on the structure factor for the polydisperse distribution given above is the plot of  $H_{a,p}(q)/H_{r,p}(q)$  for three values of the prefactor in Fig. 8. The ratio increases by about 5% as the prefactor decreases from 1.83 to 0.95, while the increase in  $A_{31}$  is about 25%. It is also seen that

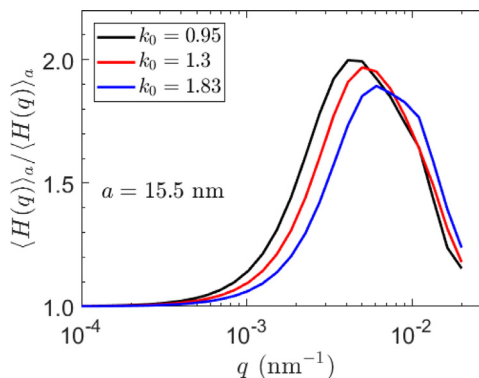


**Fig. 8.** Ratio of light scattering intensity from aligned aggregates to the intensity from randomly-oriented aggregates having a broad lognormal distribution ( $N_g=226$  and  $\sigma_g=3$ ). Results are shown for distributions involving aggregates with three different prefactors. For all cases, the fractal dimension is 1.78.

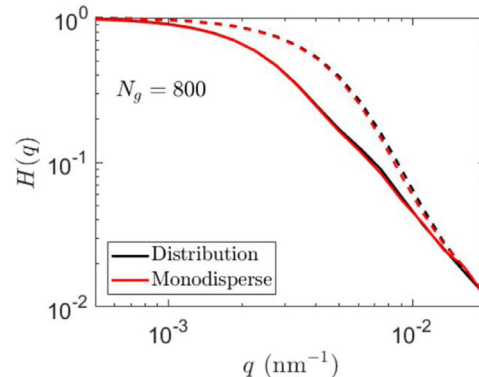
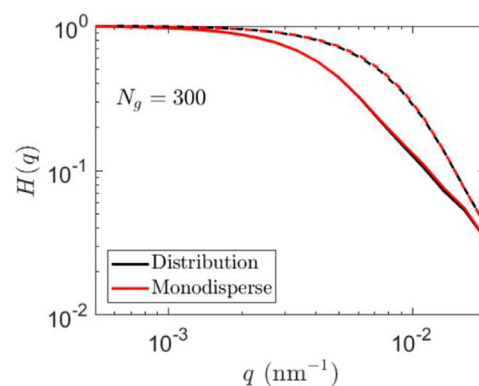


**Fig. 9.** Normalized light-scattering intensity for a narrow distribution of aggregates ( $\sigma_g=1.08$ ). Solid and dashed lines represent randomly-oriented and aligned aggregates, respectively. Results for the distributions are indistinguishable from the monodisperse cases with the number of primaries equal to  $N_g$  from the distribution.

the peak shifts to smaller  $q$  with decreasing prefactor because of the larger radius of gyration from the stringier structures. As seen in Fig. 5, the maximum structure factor ratio for the three values corresponding to the polydisperse distributions results lie below the monodisperse results.

We have also computed the light scattering intensity for the case of a more nearly monodisperse aerosol, such as the narrow distribution produced by passing a polydisperse population of aggregates through an electrical mobility classifier. (Note that we are ignoring the effects of multiply-charged particles.) As shown in Fig. 9, the structure factor for the narrow polydisperse case is almost identical with using a single value of  $N$  equal to the geometric mean number of primary spheres averaged over 20 isomers. For

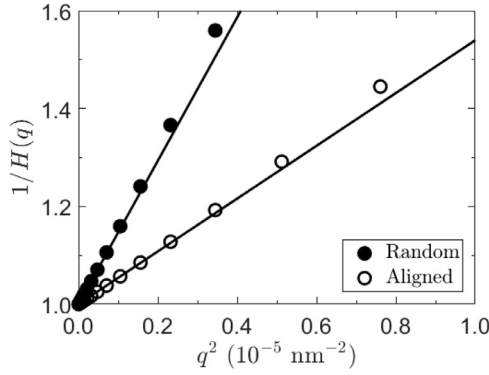


**Fig. 10.** Zimm plot for the broad distribution of aggregates ( $N_g=226$  and  $\sigma_g=3$ ). The symbols represent the results from the RDG calculations, while the solid lines represent the theoretical small  $q$  behavior for random and aligned aggregates Eqs. (18) and (19). Note that the average  $A_{31}$  and slope ratio for the distribution are 3.88 and 2.79, respectively.

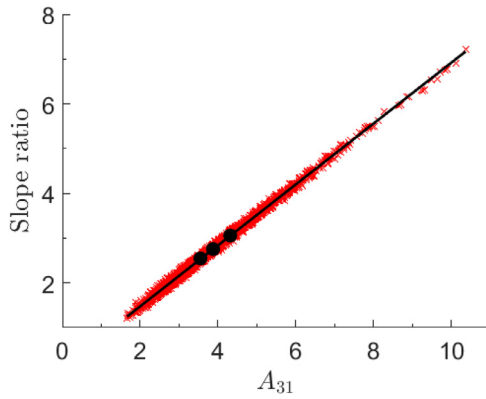


**Fig. 11.** Correlation between the slope ratio and  $A_{31}$ . The small symbols represent the values for each case in the broad size distribution (20 isomers each for 39 aggregate sizes from  $N=26$  to  $N=1946$ ). Results are shown for all three prefactors (0.95, 1.3, and 1.83) included in this study. The solid line is the best fit to the results, given by  $SR=0.680A_{31}+0.116$ . The large circles represent the average slope ratio and  $A_{31}$  for the broad distribution, with each circle representing a different prefactor. The average slope ratio and  $A_{31}$  for the distributions are defined by Eqs. (20) and (21), respectively.

the narrow polydisperse case, the distribution included 7 values of  $N$  (covering approximately 90% of the lognormal distribution) each with 20 isomers.

#### 4.5. Small angle scattering for shape anisotropy

Fig. 10 shows good agreement between the between the predicted (Eq. (19)) and computed small angle scattering Zimm plots for the broad and narrow size distributions. The simulation results exceed the model prediction with increasing  $q$  with up to 16% overestimate over the entire range and about 8% eliminating the largest values of  $q$ . The linear region moves to smaller and smaller  $q$  as the aggregate size increases for the broad distribution. The smaller range in  $q$  for linear dependence on  $q^2$  for the polydisperse case results from the dominant scattering coming from the larger aggregates.

Fig. 11 shows that there is a good correlation between the slope ratio, SR, which is the ratio of slopes  $1/H_q$  vs  $q^2$  for the random and aligned orientations, and the value of  $A_{31}$ . The solid line in the figure represents the best linear fit to the results for all aggregates in the broad size distributions (with prefactors of 0.95, 1.3, and 1.83):

$$SR = 0.680A_{31} + 0.116 \quad (22)$$

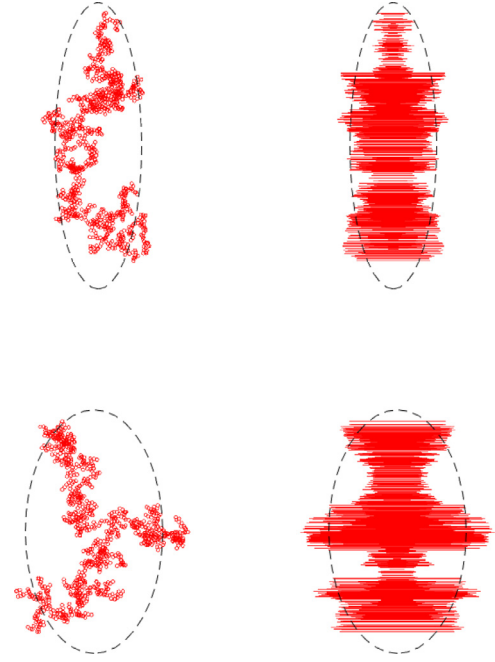


**Fig. 12.** Representation of two aggregates with  $N=1000$  monomers. The dotted line represents an equivalent prolate ellipsoid. The figures on the left show projections of each sphere in the aggregate, while the figures on the right show the center of each sphere as it is rotated around the principal axis of the polarizability tensor. Note that the aggregates at the top and bottom of the figure have  $A_{31}=6.2$  and 2.4 and  $c/\sqrt{a^2+b^2}=2.3$  and 1.3, respectively.

The standard deviation of the points relative to the best linear fit is of 0.060 with  $R^2$  for the fit equal 0.9949. It is also seen for the broad polydisperse case that the computed value for SR and the intensity weighted average value of  $A_{31}$  is close to the linear correlation.

#### 4.6. Ellipsoid representation of aggregate

It is of interest to have a geometric description of the shape parameter  $A_{31}$ . The relationships between lengths of the semi-axes ( $a > b > c$ ) of an ellipsoid with the same radii of gyration as the aggregate are given by:

$$R_{3,2}^2 = (1/5)(a^2 + b^2) \quad (23)$$

$$R_{2,2}^2 = (1/5)(a^2 + c^2) \quad (24)$$

$$R_{1,2}^2 = (1/5)(b^2 + c^2) \quad (25)$$

These three equations can be solved up to a multiplicative constant by equating the mass of the aggregate to the mass of ellipsoid.

$$(4/3)\pi r_0^3 N = (4/3)\pi abc\rho \quad (26)$$

Fig. 12 shows a comparison of the resulting ellipsoid with the aggregate coordinates. The dashed line represents the ellipse with semi-axes  $a$  and  $(b^2 + c^2)^{1/2}$ . This square root expression accounts for the orientation average about the  $a$  axis. We must know the number of primaries to obtain the ellipsoid. We can do that for the simulation. Experimentally one could estimate the number from the measured radius of gyration and the primary sphere diameter or from the aggregate mass together with the primary sphere radius.

## 5. Discussion

As discussed in Section 1, there is generally a slight difference in the direction of the aggregate for lowest energy in an electric field and the direction associated with the largest inertial eigenvalue. We have calculated SR (slope ratio) for alignment using both the polarizability and inertia tensors; the maximum difference is less than 6%, while the average difference between SR calculated with these two alignment directions is less than 1% for each aggregate size in the broad size distribution ( $N=26$  to  $N=1946$ ,  $k_0=1.3$ ). Thus, there is little difference in the small  $q$  results whether we use the polarizability or inertia tensor to compute the alignment direction. This comparison has only been made for aggregates generated by the Mackowski algorithm. We expect this result to also be true for DLCA aggregates, but we have not verified this.

Fig. 11 shows a strong correlation between the slope ratio SR computed in the small angle limit for Zimm plots and  $A_{31}$  for individual aggregates generated with the Mackowski algorithm. The theoretically predicted value of SR involves only the squares of principal radii of gyration about the various axes in the numerator and denominator and is closely related to  $A_{31}$ . These principal radii of gyration provide an overall geometric description of the aggregate that appears to be independent of the detailed fractal structure. For example, in a more realistic simulation of aggregate growth based on DLCA [25], the slopes of SR vs  $A_{31}$  (0.671 for 227 clusters with 30 spheres each and 0.675 for 137 clusters of 300 spheres each) were within about 1% of the value for Fig. 11 (0.680, see Eq. (22)). It is also of interest that the 3 values of SR vs  $A_{31}$  computed for a broad distribution of aggregates, such as observed downstream of a buoyant turbulent diffusion flame (Koylu), are in line with the correlation plot in Fig. 10. This suggests that small angle measurements would be a good way to monitor the intensity weighted value of  $A_{31}$  and also allow one to estimate the three principal radii.

The larger the aggregate, the smaller the scattering angle required to measure the slope from the Zimm plot. In Mulholland et al. [25], the estimated minimum angle required to have three evenly spaced points in terms of  $q^2$  would be  $2^\circ$  for clusters with 1000 spheres ( $R_g=630$  nm) and  $1^\circ$  for clusters with 1830 spheres ( $R_g=880$  nm). This estimate is based on a wavelength of 630 nm, a primary sphere radius of 15.5 nm,  $d_f=1.78$ , and  $k_0=1.3$ . Wang et al. [28] have carried out aerosol measurements at angles as small as this with a system that could be modified to include an electric field. Performing  $S(q)$  measurements for narrowly distributed aggregates will be challenging because of the small scattering intensity; however, the interpretation of the results will be more quantitative. It may also be possible to measure  $S(q)$  of single clusters over a time interval small compared to the rotation time of 1–5 ms for the smoke agglomerates studied by Colbeck et al. [5] and Weiss et al. [29]. Such scattering measurements have been made on individual polystyrene spheres as small as 0.2  $\mu\text{m}$  by Dick [7] and by Wyatt Aerosol Systems [2]. These measurement would provide a nearly direct comparison of the structure factor without orientation averaging.

Small angle measurements could provide tests of DLCA shape calculations by Fry et al. [9] for soot aggregates and Jullien's theory [14] on the effect of the polarizability on aggregate shape for aerosol aggregates. An extreme case of interest would be the flame-generated  $\text{Fe}_2\text{O}_3$  chain aggregates with aspect ratios as large as 40 [3,10]. Other aerosol systems where small angle measurements would be useful for shape changes are the effect of sintering for metal aggregates such as silver [15], and the effect of coatings on soot aggregates [1,27].

As discussed in the Introduction, previous studies have established the feasibility of obtaining light scattering data from iron

oxide chains at about  $30^\circ$  and for an integrated signal for soot from about  $8^\circ$  to  $172^\circ$  for aligned soot. It is likely that differential light scattering measurements of aligned aggregates can be made over the range  $10^\circ$  to  $160^\circ$ , since light scattering measurements have been made on unaligned soot over this range [18]. Such measurements would allow the determination of  $\max[\langle S(q) \rangle_a / \langle S(q) \rangle_r]$  for aggregates of about 50 spheres to more than 2000 based on a primary sphere radius of 15.5 nm and a wavelength of 630 nm. We believe that the correlation between this intensity ratio and  $A_{31}$  (Fig. 5) is strong enough to be useful in monitoring the shape of aggregates though not as strong or as directly related to the shape parameter  $A_{31}$  as the small angle measurements.

Heinson et al. [13] relate the shape factor to the stretched exponent  $\gamma$  in their three parameter characterization of fractal aggregates. They use a bottom-up approach starting with the pair correlation function that depends on only the radial distance between all the spheres in the aggregate. Such an approach does not allow one to compute the structure factor for an aligned cluster that rotates in only one direction such as shown in Fig. 4 for 20 clusters with the same number of primary spheres. To do such a calculation requires the 3-dimensional pair correlation function. In our approach, we calculate the structure factor as a function of the aggregate orientation and then average over either one angle for the aligned orientation or all three Euler angles for the random orientation. We then look for features in the  $q$  dependence of the structure factor that correlate with  $A_{31}$ . For small  $q$  a direct correlation is found. For large  $q$  an intensity ratio is found that correlates with  $A_{31}$ . This is an empirical approach treating the simulation like an experiment. There is a need to elucidate the properties of the 3-D pair correlation function that determine the structure factor in analogy to what Heinson et al. have carried out for the scalar pair correlation function. The value of  $A_{31}$  provides an overall shape factor; however, it is based on a uniform density. A full description of the shape requires the 3-D pair correlation function.

## 6. Conclusions

A linear correlation was obtained for small  $q$  between the slope ratio SR (obtained from Guinier plots for the structure factor  $S(q)$ ) and the shape parameter  $A_{31}$  for individual aggregates with fractal dimension of 1.78 and aggregate sizes ranging from 26 to 1946 spheres. The slope ratio is within 1% of the correlation obtained by Mulholland et al. [25] based on aggregates generated by DLCA simulations. For polydisperse distributions of aggregates similar to that of soot ( $N_g=226$  and  $\sigma_g=3$ ) for 3 values of the prefactor, the computed values of SR and the average of  $A_{31}$  (see caption for Fig. 11) fall on the correlation line. The results obtained for the narrowly distributed aggregates characteristic of mobility or mass classification are nearly identical to the results obtained for single value of  $N$  averaged over 20 isomers.

For the above aggregate range, the direction of the lowest dipole-field interaction energy and the direction associated with the smallest inertial eigenvalue are typically within a few degrees. This result is crucial to obtaining a strong correlation between the ratio of slopes and  $A_{31}$ . The reason for the good agreement for the direction of the principle axes of the inertial and polarizability tensor is worthy of more study.

A correlation is obtained between the maximum structure factor ratio (i.e. the peak value in a plot of  $\langle S(q) \rangle_a / \langle S(q) \rangle_r$ ) for all aggregates in the broad particle size distribution (20 isomers each for 39 aggregate sizes) vs.  $A_{31}$  for each aggregate. The peak in the structure factor ratio corresponds to the fractal range for  $q$  in terms of the randomly oriented aggregates. For some experiments, this may be a more convenient range of  $q$  compared to the small  $q$  range, which has a stronger correlation to the aggregate shape.

Previous measurements [3,5,29] have demonstrated that it is feasible to measure the light scattering intensity alternately of aligned and randomly oriented aggregates at a frequency of at least 10 Hz. Our analysis indicates that these measurements can be expanded to provide the  $q$  dependence of the structure factor for both small (Guinier regime) and large  $q$  (fractal regime). The potential for new insight of aggregate shapes is a major impetus of this paper. It is likely that such measurements would be more sensitive to aggregate shape than mobility measurements.

Two geometric representations of the overall aggregate structure are presented. Both are derived from the principle moments of inertia of the aggregates. Measurements of the light scattering intensity for small  $q$  are shown to be related to these principle moments of inertia.

Previous studies of shape have focused on the randomly oriented aggregate. We have shown that more detailed shape information is obtained by including both aligned and random orientations. The basic difference between the two orientations is that the aligned structure factor is a vector quantity related to the 3-D pair correlation function while the random structure factor is a scalar related to the scalar pair correlation function.

### Supplementary materials

Supplementary material associated with this article can be found, in the online version, at doi:10.1016/j.jqsrt.2018.07.019.

### References

- [1] Bueno P, Havey D, Gillis K, Hodges J, Mulholland G, Dickerson R, Zachariah MR. Amplification of the optical absorption cross section of soot aerosol with a nonabsorbing coating from photoacoustic measurements. *Aerosol Sci Technol* 2011;45:1217.
- [2] Cannell, D., Seifter, J., and Wyatt, P.J. (2017) Internal report by aerosol systems LLC.
- [3] Chen MT, Xie GW, Yang M, Shaw DT. Experimental characterization of chain-aggregate aerosol by electrooptic scattering. *Aerosol Sci Technol* 1991;14:74–81.
- [4] Chen SC, Wang J, Fissan H, Pui DYH. Exposure assessment of nanosized engineered agglomerates and aggregates using nuclepore filter. *J Nanopart Res* 2013;15:1955–70.
- [5] Colbeck I, Atkinson B, Johart Y. The morphology and optical properties of soot-produced by different fuels. *J Aerosol Sci* 1997;28:715–23.
- [6] Corson J, Mulholland GW, Zachariah MR. The effect of electric field induced alignment on the electrical mobility of fractal aggregates. *Aerosol Sci Technol* 2018;52:524–35.
- [7] Dick, W.D. (2006). Internal report by MSP Corp on multi-angle light scattering photometer, Shoreview, MN.
- [8] Friedlander SK. *Smoke, dust, and haze, fundamentals of aerosol dynamics*. Oxford, England: Oxford University Press; 2000.
- [9] Fry D, Mohammad A, Chakrabarti A, Sorensen CM. Cluster shape anisotropy in irreversibly aggregating particulate systems. *Langmuir* 2004;20:7871.
- [10] Fuchs NA. *The mechanics of aerosols*, New York, NY: Pergamon Press; 1964. distributed in the Western Hemisphere by Macmillan.
- [11] Goldstein H. *Classical mechanics*. Reading, MA: Addison-Wesley; 1950.
- [12] Guinier A. La diffraction des rayons x aux trespetits angles: application a l'etude de phenomes ultramicroscopiques. *Ann Phys* 1939;12:161–237.
- [13] Heinson WR, Sorensen CM, Chakrabarti A. A three parameter description of the structure of diffusion limited cluster fractal aggregates. *J. Colloid Interface Sci* 2012;375:65–9.
- [14] Jullien R. Comment on "diffusion-limited aggregation in two dimensions". *Phys Rev Lett* 1985;55:1697.
- [15] Kim SC, Wang J, Emery MS, Shin WG, Mulholland GW, Pui DYH. Structural property effect of nanoparticle agglomerates on particle penetration through fibrous filters. *Aerosol Sci. Technol.* 2009;43:344–55.
- [16] Kousaka Y, Endo Y, Ichitsubo H, Alonso M. Orientation-specific dynamic shape factors for doublets and triplets of spheres in the transition regime. *Aerosol Sci Technol* 1996;24:36–44.
- [17] Köylü ÜÖ, Faeth GM. Structure of overfire soot in buoyant turbulent diffusion flames at long residence time. *Combustion and Flame* 1992;89:140–56.
- [18] Köylü ÜÖ, Faeth GM. Optical Properties of overfire soot in buoyant turbulent diffusion flames at long residence time. *ASME J Heat Transf* 1994;116:152–9.
- [19] Li M, Mulholland GW, Zachariah MR. The effect of orientation on the mobility and dynamic shape factor of charged axially symmetric particles in an electric field. *Aerosol Sci Technol* 2012;46(9):1035–44.
- [20] Li M, Mulholland GW, Zachariah MR. Understanding the mobility of nonspherical particles in the free molecular regime. *Phys Rev E* 2014;89(2):022112.
- [21] Li M, Mulholland GW, Zachariah MR. The effect of alignment on the electric mobility of soot. *Aerosol Sci Technol* 2016;50(10):1003–16.
- [22] Lindsay HM, Klein R, Weitz DA, Lin MY, Meakin P. Structure and anisotropy of colloidal aggregates. *Phys Rev A* 1989;39:312–19.
- [23] Mackowski DW. Monte Carlo simulation of hydrodynamic drag and thermophoresis of fractal aggregates of spheres in the free-molecule flow regime. *J Aerosol Sci* 2006;37(3):242–59.
- [24] Mansfield ML, Douglas JF, Garboczi EJ. Intrinsic viscosity and the electrical polarizability of arbitrarily shaped objects. *Phys Rev E* 2001;64(6):061401.
- [25] Mulholland GW, Zhou L, Zachariah MR, Heinson WR, Chakrabarti A, Sorensen C. Light scattering shape diagnostics for nano-agglomerates. *Aerosol Sci Technol* 2013;47:520–9.
- [26] Radney JG, Zangmeister CD. Practical limitations of aerosol separation by a tandem differential mobility analyzer–aerosol particle mass analyzer. *Aerosol Sci Technol* 2016;50:160–72.
- [27] Schnitzler EG, Dutt A, Charbonneau AM, Olfert JS, Jäger W. Soot aggregate restructuring due to coatings of secondary organic aerosol derived from aromatic precursors. *Environ Sci Technol* 2014;48(24):14309–16.
- [28] Wang Y, Chakrabarti A, Sorensen CM. A light-scattering study of the scattering matrix elements of Arizona road dust. *J Quant Spectrosc Radiat Transf* 2015;163:72–9. doi:10.1016/j.jqsrt.2015.05.002.
- [29] Weiss RE, Kapustin VN, Hobbs PV. Chain-aggregate aerosols in smoke from the Kuwait oil fires. *J Geophys Res* 1992;97 14,527–14,531.
- [30] Zelenyuk A, Imre D. On the effect of particle alignment in the DMA. *Aerosol Sci Tech* 2007;41:112–24.
- [31] Sorensen CM. Light scattering by fractal aggregates: a review. *Aerosol Sci Tech* 2001;35(2):648–87.